# The Unfolding Journey of Superoxide Dismutase 1 Barrels Under Crowding: Atomistic Simulations Shed Light on Intermediate States and Their Interactions With Crowders

Stepan Timr, David Gnutt, Simon Ebbinghaus, Fabio Sterpone

# The Unfolding Journey of Superoxide Dismutase 1 Barrels under Crowding: Atomistic Simulations Shed Light on Intermediate States and Their Interactions with Crowders

Stepan Timr,[*,†,‡] David Gnutt,[¶,§] Simon Ebbinghaus,[¶,§] and Fabio Sterpone[*,†,‡]

†*CNRS, Université de Paris, UPR 9080, Laboratoire de Biochimie Théorique, 13 rue Pierre et Marie Curie, F-75005, Paris, France*

‡*Institut de Biologie Physico-Chimique-Fondation Edmond de Rothschild, PSL Research University, Paris, France*

¶*Institute of Physical and Theoretical Chemistry, Technical University Braunschweig, Rebenring 56, 38106 Braunschweig, Germany*

§*Department of Physical Chemistry II, Ruhr University Bochum, Universitätsstrasse 150, 44801 Bochum, Germany*

E-mail: timr@ibpc.fr; fabio.sterpone@ibpc.fr

**Abstract**

The thermal stability of the superoxide dismutase 1 protein in a crowded solution is investigated by performing enhanced sampling molecular simulations. By complementing thermal unfolding experiments done close to physiological conditions (200 mg/mL), we provide evidence that the presence of the protein crowder bovine serum albumin in different packing states has only a minor, and essentially destabilizing, effect. The finding that quinary interactions counteract the pure stabilization contribution stemming from excluded volume is rationalized here by exploring the SOD1 unfolding mechanism in microscopic detail. In agreement with recent experiments, we unveil the importance of intermediate unfolded states as well as the correlation between protein conformations and local packing with the crowders. This link helps us to elucidate why certain SOD1 mutations involved in the ALS disease reverse the stability effect of the intracellular environment.

# Graphical TOC Entry

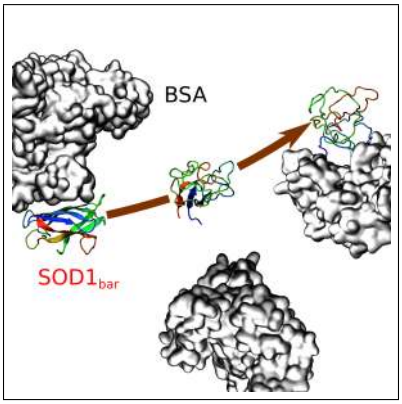


# Keywords

superoxide dismutase 1, thermal stability, macromolecular crowding, mutations, molecular simulations

In living cells, proteins are exposed to a highly crowded and heterogeneous environment.[1] These crowded conditions can affect the stability of a protein owing to a combined effect of excluded volume and weak transient (quinary) interactions with the surroundings. Whether the net effect is stabilizing, or destabilizing depends on the composition of the environment and on the protein sequence.[2–7] Destabilization of the native fold of a protein, potentially followed by aggregation and fibril formation, was linked to numerous diseases and pathological states.[8,9] This is also the case of superoxide dismutase 1 (SOD1), an enzyme abundantly found in the interior of mammalian cells.[10–12] Multiple mutations in SOD1 have been associated with the familial form of amyotrophic lateral scleroris (fALS).[10] In its mature state, SOD1 is a stable homodimer of two $\beta$-barrels, which constitute an active site sequestering a copper and a zinc ion. In contrast, immature, metal-depleted forms of SOD1 favor a less stable monomeric state under physiological conditions,[13,14] and a likely precursor of aberrant oligomers and fibrils.[15–18] How the crowded environment inside cells affects the destabilization, misfolding, and aggregation of SOD1 is not yet clear. Experimental works[5,7] addressing the stability of loop-truncated SOD1 monomers ($SOD1_{bar}$, see Figure 1) under crowding found that the monomers can be weakly destabilized by the intracellular environment as well as by protein solutions (lysozyme, BSA). In a recent study[7] that combined in-cell unfolding thermodynamic studies using fast relaxation imaging (FReI)[19] with multi-scale molecular simulations[20,21], we showed that the destabilizing effect of the crowded environment can be reverted by a single-point mutation. Moreover, we established a link between $SOD1_{bar}$ conformations, the interactions with the crowders, and the effects of single-point mutations[7]. Here we use a fully atomistic model in explicit solvent to examine the thermal stability of $SOD1_{bar}$ in a crowded environment formed by a solution of bovine serum albumin (BSA). Namely, we present the results of enhanced sampling simulations based on the REST2 technique[21,22] which were performed on two typical packing states of $SOD1_{bar}$ sampled in a crowded BSA solution (see Methods in SI) and which were compared with the dilute solution case. The packing states contained either one, or two BSA molecules

(1:1 and 2:1 packing, see Figure 1). The total simulation time for each REST2 simulation reached 24x0.5 $\mu$s. Our study, which complements past work on SOD1 stability based on lower resolution approaches,[23–29] confirms the experimental slight effect of crowding on the $SOD1_{bar}$ stability and allows us to identify intermediate states during the thermal unfolding that might be relevant for pathological aggregation.

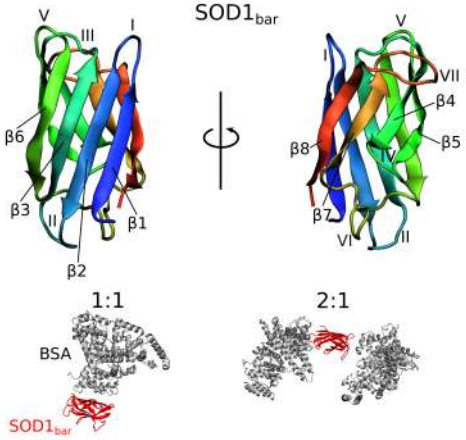


Figure 1: (Top) The crystal structure of $SOD1_{bar}$[30] with its beta strands $\beta1$–$\beta8$ and loops I–VII. $SOD1_{bar}$ is a truncated variant of the SOD1 monomer with shortened active-site loops, which retains the folding characteristics of the full-length monomer[31] and, while providing several experimental advantages[31,32], it allows investigating many disease-related mutations that affect the stability of the full-length protein[33]. (Bottom) Two states of local packing around $SOD1_{bar}$ which were extracted from a Lattice Boltzmann Molecular Dynamics (LBMD) simulation in 200 g/L BSA[7] and used for the REST2 simulations presented in this article.

*Thermal stability.* As anticipated, our simulations revealed only a weak dependence of $SOD1_{bar}$ thermal stability on the crowding state. This finding is consistent with FReI measurements of the stability of $SOD1_{bar}$ in 200 g/L BSA, reporting only a small decrease in the melting temperature by 5 ± 2 K and a small decrease in the unfolding free energy $\Delta G_u$ at 310 K by 0.4 ± 0.3 kcal/mol (see Table S1 in SI). From our simulations, we quantified the foldedness of $SOD1_{bar}$ by means of two observables, the fraction $Q_N$ of native contacts and the overall secondary structure content $Q_S$ (see Methods in SI for details). The dependence of $Q_N$ and $Q_S$ on the temperature for both packing states and for dilute conditions is shown in Figure 2A,B. From these quantities, we reconstructed the free energies $\Delta G_u(T)$ of unfolding

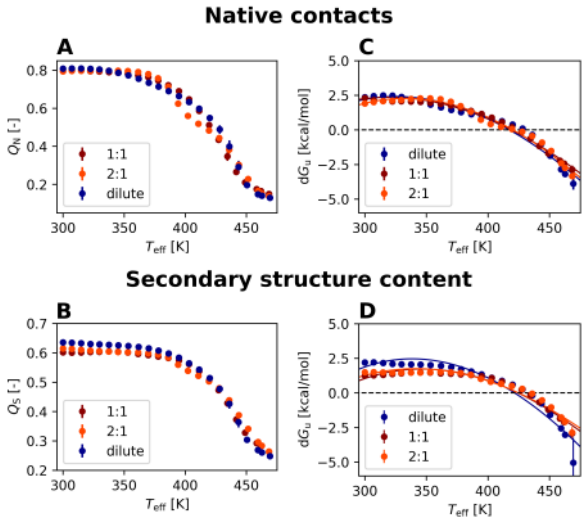


Figure 2: Thermal stability of $\mathrm{SOD1_{bar}}$ in the different crowding states, expressed (**A**) by means of the fraction of native contacts $Q_\mathrm{N}$ and (**B**) as the fraction of $\mathrm{SOD1_{bar}}$ secondary structure content $Q_\mathrm{S}$. (**C**, **D**) Free energies of unfolding derived from **A** and **B**, respectively, using a two-state model and fitted with the Gibbs-Helmholtz equation (solid lines); see SI for more details. The error bars in each plot represent standard errors of the mean of values obtained from 50 ns intervals.

using a two-state model (Figure 2C,D). As can be seen from the plots, the two observables $Q_\mathrm{N}$ and $Q_\mathrm{S}$ consistently indicate that the different crowding conditions do not lead to a strong difference in thermal stability. In fact, the melting temperatures, derived as the temperatures where $\Delta G_\mathrm{u}(T) = 0$, agreed within the error bars for the different systems (see Tables S2 and S3 in SI). Note that the thermal unfolding of crowders is not considered in the present simulations scheme as their temperature is maintained at 300 K. Close to ambient temperature we observe a slight destabilization due to crowding, an effect that is more pronounced when considering the $Q_\mathrm{S}$ parameter (Figs. 2B,D).

*Intermediate states.* A closer look at the native contact distributions sampled in the different REST2 simulations unveils the presence of intermediate states between the fully folded and fully unfolded states (Figure 3). In fact, a four-state model yields a better fit of the $Q_\mathrm{N}$ dependence than a two-state model (see Figure S2 in SI). Previous ensemble-based experimental measurements concluded that the folded–unfolded transition of SOD1 monomers is cooperative and consistent with a two-state model.[5,31] However, recent single-molecule

folding experiments,[34] reported a more complex behavior and highlighted the importance of intermediate states. The results of our simulations point in the same direction, see Figures S3–S5 in SI. Despite specificities, all the three simulated systems provide a consistent view of the unfolding process: First of all, we observe geometries ($Q_{\mathrm{N}} = 0.5-0.7$) where the $\beta$-barrel maintains its overall integrity but localized deformations affect the region of the $\beta$-strands $\beta5$ and $\beta6$, which appear as the weak spot for thermal unfolding. Moreover, in agreement with NMR study[31], we report the tendency of $\beta5$ to shift toward $\beta6$. Interestingly, simulations of mechanical unfolding[35] reported that the same region has high resistance to the unfolding force. This highlights the non-equivalency of thermal and mechanical unfolding, which was already described in the literature.[36,37] As the thermal unfolding progresses ($Q_{\mathrm{N}} = 0.2-0.5$), the structure of the the $\beta$-barrel becomes strongly perturbed. Specifically, the side of the barrel consisting of $\beta5$, $\beta4$, and $\beta7$, forming the dimer interface in the full-length SOD1, progressively disintegrates, the unfolded $\beta5$ can detach from the barrel surface and create a loop outside the barrel, and $\beta8$ can swap its position with $\beta7$. These findings are in line with previous experiments[15,38] and simulations[25,28] on full-length SOD1, which identified this side of the $\beta$-barrel to be more dynamic than the opposite surface. Only beta strands $\beta1$–$\beta3$ remain folded in certain structures, which confirms the observation from single-molecule folding experiments,[34] identifying strands $\beta1$ to $\beta3$ as a stable core of the barrel. Finally, at $Q_{\mathrm{N}} = 0 - 0.2$, the unfolding is essentially complete, with some geometries containing short $\beta$-strand or $\alpha$-helical segments. Our finding that crowding does not dramatically alter the process of SOD1 unfolding agrees with previous Monte Carlo (MC) simulations of the initial stages of full-length SOD1 unfolding in crowded conditions.[28] It must be considered that the relative populations of the observed intermediates states might be biased by the finite timescale of our simulations.

*Unfolding alters interactions with crowders.* At a given temperature, fully or partially unfolded states tend to interact with BSA more than the folded structures (see Fig. 4A). This observation confirms previous insights from experiments[5] about quinary interactions

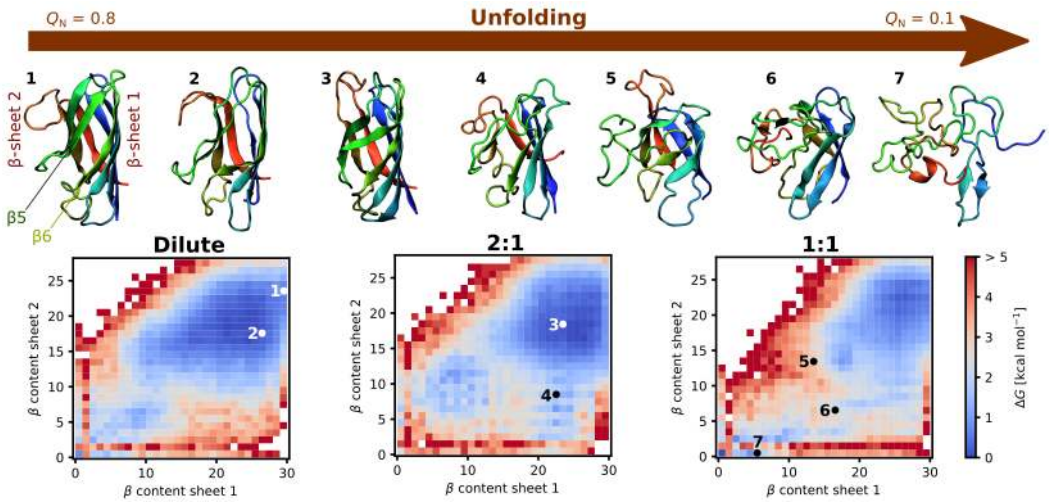


Figure 3: (Top) Representative $SOD1_{bar}$ structures along the unfolding pathway: (1) native state, (2) the region of $\beta5$, $\beta6$, and $\beta8$ starts to unfold, (3) $\beta5$ bridges the opening toward $\beta6$, (4) the side of the barrel consisting of $\beta5$, $\beta4$, and $\beta7$ disintegrates, (5) transient smaller $\beta$-barrel with $\beta5$ forming a loop outside, (6) strongly unfolded conformation with the region $\beta1$-$\beta3$ being the last to withstand unfolding, (7) fully unfolded conformation containing some residual secondary structure. (Bottom) Free-energy landscapes of $SOD1_{bar}$ unfolding in the different crowding states near melting ($T_{eff}$ =427–428 K). The collective variables express the number of residues with the $\beta$-sheet secondary structure in each of the two $\beta$-sheets forming the barrel, namely $\beta$-sheet 1 (consisting of $\beta$-strands $\beta1$, $\beta2$, $\beta3$, and $\beta6$) and $\beta$-sheet 2 ($\beta4$, $\beta5$, $\beta7$, and $\beta8$). The free-energy surfaces rendered for all temperatures can be found in SI (Figure S6).

acting primarily on the unfolded ensemble, which provides a support for the hypothesis that quinary interactions favor unfolded structures over the folded ones. For the 1:1 system, it is the fully unfolded structures that have the most contacts with the crowder. In contrast, in the simulation of the 2:1 packing, we observe the highest number of contacts for an intermediate state with a misfolded region between $\beta4$ and $\beta6$. This denaturated region has a strong propensity to interact with BSA (see Figure 4B), which suggests that interactions with BSA promote the formation of this semiunfolded intermediate state.

*Effect of loop VII conformation.* As we described in our previous work[7], the loop VII ($loop_{91-101}$), oscillates between extended and compact geometries in the folded $SOD1_{bar}$ structures (Figure 4C). We found previously that the extended loop VII geometries had more contacts with BSA than the compact ones[7]. Here we complement this observation by

noting that the extended geometries expose the dimer interface of the barrel and correlate with an increased interaction of the region $\beta$4–$\beta$6 with the crowder (see Figure 4D and Figure S8 in SI). Consequently, the increased crowder interactions of this region, which we identified as a fragile part of the $\beta$-barrel, may lead to the destabilization of the $\beta$-barrel. To see if mutations of histidine 46, which were shown to revert the destabilization by the crowded environment[7] , could alter the loop conformation and thereby change the exposure of the fragile region to crowders, we performed alchemical calculations of mutation free energies[39]. We found that the mutation of histidine 46 (H46) to serine (S), arginine (R), or phenylalanine (F) favors the more compact geometries of the loop VII over the extended ones (see Figure 4F and Figure S9 in SI). This finding suggests that the H46S/R/F mutation decreases the number of contacts of the $\beta$4-$\beta$6 region and of the loop VII with the crowder, thereby reducing the destabilizing effect. This offers a more detailed explanation of why these mutations counteract the destabilizing effect of BSA.[7]

*Contacts with crowders changed by heating.* In general, the average contact number of $SOD1_{bar}$ with BSA decreases with increasing temperature (see Figure S10A in SI), reflecting the fact that the higher kinetic energy allows $SOD1_{bar}$ to escape more easily from the potential-energy wells associated with attractive interactions with the crowder. The only exception to this otherwise general trend is a plateau or even a transient increase appearing in a region around the melting temperature (Figure S10A in SI). The existence of this transient reversal is caused by the tendency of (semi)unfolded structures to interact more with the crowder. On the other hand, the folded $\beta$-barrel detaches more often from BSA with increasing temperature, and the interaction pattern evolves toward loop-mediated interactions (see Figure S8 in SI). Even at the ambient temperature, mutual displacement of $SOD1_{bar}$ and the crowder(s) lead to a significant broadening of the contact distribution with respect to the initial configuration (Figure S8 in SI). Interestingly, when following the process of unfolding in each replica, traveling across the temperature space, we find that the surface of the $\beta$-barrel always detaches from BSA before complete unfolding (see Figure S10B in SI).

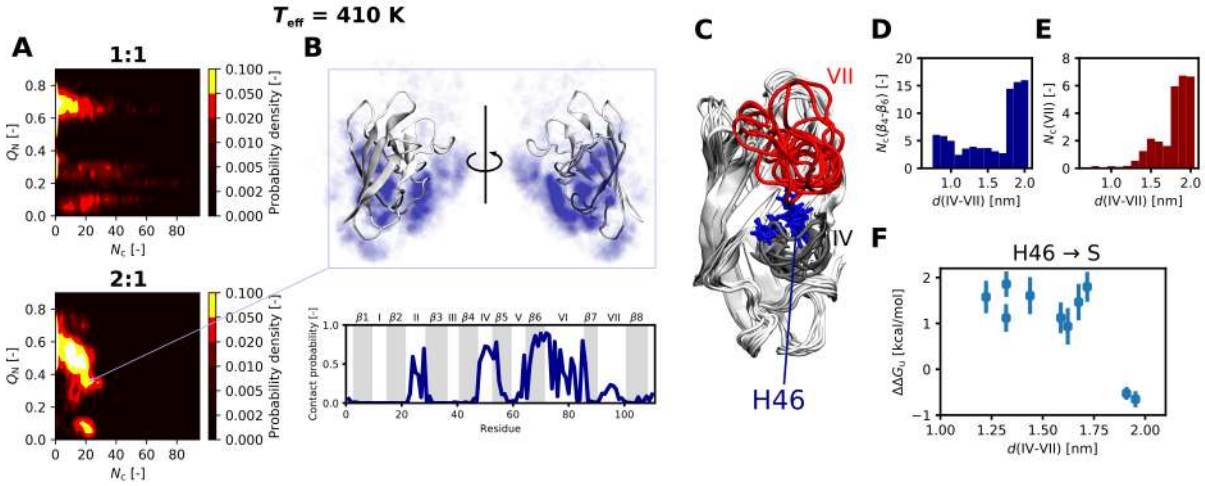


Figure 4: (**A**) Number of $\mathrm{SOD1_{bar}}$ residues in contact with BSA ($N_c$) versus the fraction of native contacts ($Q_N$) for the two crowded systems at $T_{eff}$ = 410 K. (Semi)unfolded conformations are found to interact with BSA more than folded structures. (**B**) Distribution of contacts with BSA of a partially unfolded state featuring a misfolded region between $\beta$4 and $\beta$6 in the 2:1 simulation at $T_{eff}$ = 410 K. The blue clouds around the structure of $\mathrm{SOD1_{bar}}$ depict the spatial distributions of BSA atoms interacting with $\mathrm{SOD1_{bar}}$. The data show that the denaturated region has a strong propensity to interact with BSA. (**C**) Conformational flexibility of the loops VII and IV as observed in the dilute REST2 simulation. (**D**,**E**) Distance between the loops IV and VII versus the number of residues in contact with BSA from the $\beta$4-$\beta$6 region and from the loop VII, respectively (data from the 2:1 packing at 300 K). Extended loop VII conformations lead to more contacts with BSA. (**F**) Correlation of the distance between the loops IV and VII with the change in the free energy of unfolding upon the H46S mutation. The mutation of histidine 46 to serine favors compact conformations of the loop VII.

Documenting the fact that heating changes the local packing around $\mathrm{SOD1_{bar}}$, this observation also reveals that there is a competition between unfolding kinetics and detachment from the crowders upon heating.

*Toward a thermodynamic picture.* The melting temperatures extracted from the simulations ($T_m \simeq 400$ K), are higher than the experimental values (Tables S2 and S3 in SI). In fact, our FReI measurements of $\mathrm{SOD1_{bar}}$ stability resulted in a melting temperature of $331.2 \pm 1.6$ K in dilute conditions, a value close to that derived from circular dichroism measurements.[5] This difference might be caused by limited sampling in simulations and by the widespread tendency of atomistic force fields to stabilize the native folded state relative to the unfolded ensemble.[36,40,41] Also note that due to the long time scales involved in protein

folding, it is highly unlikely to observe the re-folding of an unfolded replica in any REST2 simulation of a protein comparable in size to $SOD1_{bar}$ (see Figure S13 in SI and its caption for the visualization of replica migration and for more discussion). Nevertheless, the relative stability effect of crowding can be captured by REST2 in that the interactions with the crowders affect the migration of the unfolded replicas along the temperature ladder.

A complete description of the mechanism of (de)stabilization can be deduced from the full set of parameters of the Gibbs-Helmholtz equation: the melting temperature but also the unfolding enthalpy ($\Delta H_{\mathrm{m}}$) and the specific heat of unfolding ($\Delta C_{\mathrm{p}}$).[42] Unfortunately, the overestimation of the melting temperature could affect the apparent values of $\Delta H_{\mathrm{m}}$ and $\Delta C_{\mathrm{p}}$, extracted from the two-state fit of the stability curve. We attempted an alternative estimate by performing direct simulations as a function of temperature of a set of folded and unfolded configurations extracted from dilute REST2, and by recording the enthalpy of unfolding $\Delta H(T)$, see SI for details (e.g., Fig. S11). When interpolated to $T_{\mathrm{m}}^{\mathrm{exp}} = 331.2$ K, the value $\Delta H(T = T_{\mathrm{m}}^{\mathrm{exp}}) = 57$ kcal/mol is somewhat higher but of the same order of magnitude as the experimental results from our FReI measurements ($37 \pm 3$ kcal/mol) and from previous circular dichroism experiments ($43.7 \pm 0.7$ kcal/mol).[5] Analogous calculations for geometries sampled in the 1:1 crowded REST2 simulation resulted in $\Delta H(T = T_{\mathrm{m}}^{\mathrm{exp}}) = 63$ kcal/mol, with $T_{\mathrm{m}}^{\mathrm{exp}} = 326.4$ K corresponding to the melting temperature of $SOD1_{bar}$ in 200 g/L BSA. Thus, the simulations confirm an increase in $\Delta H_{\mathrm{m}}$ induced by the crowded environment, as suggested by experiments (see Table S1 in SI).

On the other hand, $\Delta C_{\mathrm{p}} = 0.32$ kcal/mol/K, obtained from a linear fit of the calculated enthalpy differences (Figure S11A), is significantly smaller than the experimental value ($1.55 \pm 0.05$ kcal/mol/K).[5] An analogous calculation for the crowded 1:1 system resulted in a similar value (0.27 kcal/mol/K), although more with higher uncertainty. We thus tried to rationalize this discrepancy.

The origins of the positive specific heat of unfolding are still debated,[43,44], but a dominant contribution seems to arise from an increased solvent exposure of hydrophobic groups of the

protein. We therefore computed the change in exposed surface area upon unfolding. For the dilute conditions we obtained $\Delta A_{\text{phobic}} = 5.3 \pm 0.6$ nm$^2$ and $\Delta A_{\text{philic}} = 1.1 \pm 0.7$ nm$^2$. By using a semi-empirical approach relating the changes in the hydrophobic and hydrophilic solvent-accessible surface areas with the specific heat of unfolding[43] (see Methods in SI for more details), we derived an estimate of the solvation contribution to $\Delta C_{\text{p}}$ between 0.07 and 0.25 kcal/mol/K. For comparison, we also computed the vibrational contribution to $\Delta C_{\text{p}}$ (Figure S11B in SI), obtaining the value 0.46 kcal/mol/K. Even if the two contributions are added, the obtained value is still half of the experimental estimate. This picture also holds for the crowded 1:1 system, see the data reported in Table S4 in SI. The discrepancy between *in silico* and experimental $\Delta C_{\text{p}}$ values seems to largely stem from the compactness of the unfolded state observed in simulations and reflected by the relatively small differences in the solvent-accessible surface areas upon unfolding. In fact, an additional simulation performed with an expanded unfolded state in dilute conditions yielded considerably higher estimates—reaching up to 1 kcal/mol/K—of the solvation contribution to $\Delta C_{\text{p}}$ (see Figure S12 in SI). When combined with the vibrational contribution reported above, such values result in $\Delta C_{\text{p}}$ estimates that are comparable with the experimental value[5] ($1.55 \pm 0.05$ kcal/mol/K). The tendencies of current all-atom force fields, including the ff99SB*-ILDN model employed in this study, to produce compact disordered states have already been identified in the literature[40,45].

Finally, and focusing only on the SOD1$_{\text{bar}}$ protein, it is worth noting that the difference in vibrational entropy between the folded and the fully unfolded state decreased by 25% in the crowded system (Figure S11B in SI), possibly due to interactions with the crowder constraining the dynamics of the unfolded state. Similarly, we detected a 20% decrease in the conformational entropy difference upon unfolding in the crowded system (Figure S11C in SI); for details on entropy calculations see Methods in SI.

In this work, we investigated, with an all-atomistic resolution, the thermal stability and unfolding of SOD1$_{\text{bar}}$ in a crowded environment formed by BSA. Consistent with FReI mea-

surements, we found only a mild effect of the crowders on the stability of $SOD1_{bar}$. Our simulations provided a detailed picture of $SOD1_{bar}$ unfolding, highlighting the existence of multiple intermediate states along the unfolding pathway, a finding which is consistent with recent single-molecule experiments.[34] In particular, we identified the role of the region between the beta sheets $\beta 4$ and $\beta 6$ in early stages of the unfolding process, and we related histidine 46 mutations, decreasing the interaction of this region with the crowder, to an experimentally observed reversal of destabilization by BSA. The propensity of the $\beta 4$–$\beta 6$ region to early unfolding and its frequent interactions with the crowders could form an important ingredient for understanding the misfolding and aggregation of SOD1 in the crowded cellular environment.

## Acknowledgement

This project has received funding from the European Union's Horizon 2020 research and innovation programme under the Marie Sklodowska-Curie grant agreement No 840395. The research leading to these results has received funding from the People Programme (Marie Curie Actions) of the European Union's Seventh Framework Programme (FP7/2007-2013) under REA grant agreement n. PCOFUND-GA-2013-609102, through the PRESTIGE programme coordinated by Campus France. Part of this work was performed using HPC resources from GENCI [CINES, TGCC, IDRIS] (grant x20186818). D.G. acknowledges funding from the Cluster of Excellence RESOLV (EXC 1069), the Human Frontier Science Program (RGP0022/2017), the German-Israeli Foundation for Scientific Research and Development (grant 1410), and the International Graduate School of Neuroscience (Ruhr-University Bochum).

## Supporting Information Available

Methods and additional trajectory analysis.

# References


(1) Ellis, R. J.; Minton, A. P. Join the Crowd. *Nature* **2003**, *425*, 27–28.

(2) Miklos, A. C.; Sarkar, M.; Wang, Y.; Pielak, G. J. Protein Crowding Tunes Protein Stability. *J. Am. Chem. Soc.* **2011**, *133*, 7116–7120.

(3) Dhar, A.; Girdhar, K.; Singh, D.; Gelman, H.; Ebbinghaus, S.; Gruebele, M. Protein Stability and Folding Kinetics in the Nucleus and Endoplasmic Reticulum of Eucaryotic Cells. *Biophys. J.* **2011**, *101*, 421–430.

(4) Monteith, W. B.; Cohen, R. D.; Smith, A. E.; Guzman-Cisneros, E.; Pielak, G. J. Quinary Structure Modulates Protein Stability in Cells. *Proc. Natl. Acad. Sci. U.S.A.* **2015**, *112*, 1739–1742.

(5) Danielsson, J.; Mu, X.; Lang, L.; Wang, H.; Binolfi, A.; Theillet, F.-x.; Bekei, B.; Logan, D. T.; Selenko, P.; Wennerström, H. et al. Thermodynamics of Protein Destabilization in Live Cells. *Proc. Natl. Acad. Sci. U.S.A.* **2015**, *112*, 12402–12407.

(6) Cohen, R. D.; Pielak, G. J. Electrostatic Contributions to Protein Quinary Structure. *J. Am. Chem. Soc.* **2016**, *138*, 13139–13142.

(7) Gnutt, D.; Timr, S.; Ahlers, J.; Ko, B.; Manderfeld, E.; Heyden, M.; Sterpone, F.; Ebbinghaus, S. Stability Effect of Quinary Interactions Reversed by Single Point Mutations. *J. Am. Chem. Soc.* **2019**, *141*, 4660–4669.

(8) Thomas, P. J.; Qu, B. H.; Pedersen, P. L. Defective Protein Folding as a Basis of Human Disease. *Trends Biochem. Sci.* **1995**, *20*, 456–459.

(9) Owen, M. C.; Gnutt, D.; Gao, M.; Wärmländer, S. K. T. S.; Jarvet, J.; Gräslund, A.; Winter, R.; Ebbinghaus, S.; Strodel, B. Effects of in vivo Conditions on Amyloid Aggregation. *Chem. Soc. Rev.* **2019**, *48*, 3946–3996.

(10) Pasinelli, P.; Brown, R. H. Molecular Biology of Amyotrophic Lateral Sclerosis: Insights from Genetics. *Nat. Rev. Neurosci.* **2006**, *7*, 710–723.

(11) Rakhit, R.; Chakrabartty, A. Structure, Folding, and Misfolding of Cu, Zn Superoxide Dismutase in Amyotrophic Lateral Sclerosis. *Biochim. Biophys. Acta - Molecular Basis of Disease* **2006**, *1762*, 1025–1037.

(12) Johnston, J. A.; Dalton, M. J.; Gurney, M. E.; Kopito, R. R. Formation of High Molecular Weight Complexes of Mutant Cu, Zn-Superoxide Dismutase in a Mouse Model for Familial Amyotrophic Lateral Sclerosis. *Proc. Natl. Acad. Sci. U.S.A.* **2000**, *97*, 12571–12576.

(13) Arnesano, F.; Banci, L.; Bertini, I.; Martinelli, M.; Furukawa, Y.; Halloran, T. V. O. The Unusually Stable Quaternary Structure of Human Cu,Zn-Superoxide Dismutase 1 is Controlled by Both Metal Occupancy and Disulfide Status. *J. Biol. Chem.* **2004**, *279*, 47998–48003.

(14) Culik, R. M.; Sekhar, A.; Nagesh, J.; Deol, H.; Rumfeldt, J. A. O.; Meiering, E. M.; Kay, L. E. Effects of Maturation on the Conformational Free-Energy Landscape of SOD1. *Proc. Natl. Acad. Sci. U.S.A.* **2018**, *115*, E2546–E2555.

(15) Teilum, K.; Smith, M. H.; Schulz, E.; Christensen, L. C.; Solomentsev, G.; Oliveberg, M.; Akke, M. Transient Structural Distortion of Metal-Free Cu/Zn Superoxide Dismutase Triggers Aberrant Oligomerization. *Proc. Natl. Acad. Sci. U.S.A.* **2009**, *106*, 18273–18278.

(16) Sirangelo, I.; Iannuzzi, C. The Role of Metal Binding in the Amyotrophic Lateral Sclerosis-Related Aggregation of Copper-Zinc Superoxide Dismutase. *Molecules* **2017**, *22*, 1–13.

(17) Khan, M. A. I.; Respondek, M.; Kjellstro, S.; Deep, S.; Linse, S.; Akke, M. Cu/Zn Superoxide Dismutase Forms Amyloid Fibrils under Near-Physiological Quiescent Con-

ditions: The Roles of Disulfide Bonds and Effects of Denaturant. *ACS Chem. Neurosci.* **2017**, *8*, 2019–2026.

(18) Zhu, C.; Beck, M. V.; Griffith, J. D.; Deshmukh, M.; Dokholyan, N. V. Large SOD1 Aggregates, Unlike Trimeric SOD1, Do Not Impact Cell Viability in a Model of Amyotrophic Lateral Sclerosis. *Proc. Natl. Acad. Sci. U.S.A.* **2018**, *115*, 4661–4665.

(19) Ebbinghaus, S.; Dhar, A.; McDonald, J. D.; Gruebele, M. Protein folding stability and dynamics imaged in a living cell. *Nat. Methods* **2010**, *7*, 319–323.

(20) Sterpone, F.; Derreumaux, P.; Melchionna, S. Protein Simulations in Fluids: Coupling the OPEP Coarse-Grained Force Field with Hydrodynamics. *J. Chem. Theory Comput.* **2015**, *11*, 1843–1853.

(21) Stirnemann, G.; Sterpone, F. Recovering Protein Thermal Stability Using All-Atom Hamiltonian Replica-Exchange Simulations in Explicit Solvent. *J. Chem. Theory Comput.* **2015**, *11*, 5573–5577.

(22) Wang, L.; Friesner, R. A.; Berne, B. J. Replica Exchange with Solute Scaling : A More Efficient Version of Replica Exchange with Solute Tempering (REST2). *J. Phys. Chem. B* **2011**, *115*, 9431–9438.

(23) Ding, F.; Dokholyan, N. V. Dynamical Roles of Metal Ions and the Disulfide Bond in Cu, Zn Superoxide Dismutase Folding and Aggregation. *Proc. Natl. Acad. Sci. U.S.A.* **2008**, *105*, 19696–19701.

(24) Proctor, E. A.; Ding, F.; Dokholyan, N. V. Structural and Thermodynamic Effects of Post-translational Modifications in Mutant and Wild Type Cu, Zn Superoxide Dismutase. *J. Mol. Biol.* **2011**, *408*, 555–567.

(25) Ding, F.; Furukawa, Y.; Nukina, N.; Dokholyan, N. V. Local Unfolding of Cu, Zn

Superoxide Dismutase Monomer Determines the Morphology of Fibrillar Aggregates. *J. Mol. Biol.* **2012**, *421*, 548–560.

(26) Habibi, M.; Rottler, J.; Plotkin, S. S. The Unfolding Mechanism of Monomeric Mutant SOD1 by Simulated Force Spectroscopy. *Biochim. Biophys. Acta - Proteins and Proteomics* **2017**, *1865*, 1631–1642.

(27) Peng, X.; Cashman, N. R.; Plotkin, S. S. Prediction of Misfolding-Specific Epitopes in SOD1 Using Collective Coordinates. *J. Phys. Chem. B* **2018**, *122*, 11662–11676.

(28) Bille, A.; Jensen, K. S.; Mohanty, S.; Akke, M.; Irbäck, A. Stability and Local Unfolding of SOD1 in the Presence of Protein Crowders. *J. Phys. Chem. B* **2019**, *123*, 1920–1930.

(29) Mouro, P. R.; Paula, A.; Povinelli, R.; Leite, V. B. P.; Chahine, J. Exploring Folding Aspects of Monomeric Superoxide Dismutase. *J. Phys. Chem. B* **2020**,

(30) Danielsson, J.; Awad, W.; Saraboji, K.; Kurnik, M.; Lang, L.; Leinartaite, L.; Marklund, S. L.; Logan, D. T.; Oliveberg, M. Global Structural Motions from the Strain of a Single Hydrogen Bond. *Proc. Natl. Acad. Sci. U.S.A.* **2013**, *110*, 3829–3834.

(31) Danielsson, J.; Kurnik, M.; Lang, L.; Oliveberg, M. Cutting off Functional Loops from Homodimeric Enzyme Superoxide Dismutase 1 (SOD1) Leaves Monomeric $\beta$-Barrels. *J. Biol. Chem.* **2011**, *286*, 33070–33083.

(32) Danielsson, J.; Inomata, K.; Murayama, S.; Tochio, H.; Lang, L.; Shirakawa, M.; Oliveberg, M. Pruning the ALS-Associated Protein SOD1 for in-Cell NMR. *J. Am. Chem. Soc.* **2013**, *135*, 10266–10269.

(33) Lindberg, M. J.; Bystrom, R.; Boknas, N.; Andersen, P. M.; Oliveberg, M. Systematically Perturbed Folding Patterns of Amyotrophic Lateral Sclerosis (ALS)-Associated SOD1 Mutants. *Proc. Natl. Acad. Sci. U.S.A.* **2005**, *102*, 9754–9759.

(34) Sen Mojumdar, S.; N. Scholl, Z.; Dee, D. R.; Rouleau, L.; Anand, U.; Garen, C.; Woodside, M. T. Partially Native Intermediates Mediate Misfolding of SOD1 in Single-Molecule Folding Trajectories. *Nat. Commun.* **2017**, *8*, 1881.

(35) Habibi, M.; Rottler, J.; Plotkin, S. S. As Simple As Possible, but Not Simpler: Exploring the Fidelity of Coarse-Grained Protein Models for Simulated Force Spectroscopy. *PLOS Comput. Biol.* **2016**, *12*, 1–31.

(36) Stirnemann, G.; Sterpone, F. Mechanics of Protein Adaptation to High Temperatures. *J. Phys. Chem. Lett.* **2017**, *8*, 5884–5890.

(37) Languin-Cattoën, O.; Melchionna, S.; Derreumaux, P.; Stirnemann, G.; Sterpone, F. Three Weaknesses for Three Perturbations: Comparing Protein Unfolding under Shear, Force, and Thermal Stresses. *J. Phys. Chem. B* **2018**, *122*, 11922–11930.

(38) Doyle, C. M.; Rumfeldt, J. A.; Broom, H. R.; Sekhar, A.; Kay, L. E.; Meiering, E. M. Concurrent Increases and Decreases in Local Stability and Conformational Heterogeneity in Cu, Zn Superoxide Dismutase Variants Revealed by Temperature-Dependence of Amide Chemical Shifts. *Biochemistry* **2016**, *55*, 1346–1361.

(39) Seeliger, D.; de Groot, B. L. Protein Thermostability Calculations Using Alchemical Free Energy Simulations. *Biophys. J.* **2010**, *98*, 2309–2316.

(40) Piana, S.; Klepeis, J. L.; Shaw, D. E. Assessing the Accuracy of Physical Models Used in Protein-Folding Simulations: Quantitative Evidence from Long Molecular Dynamics Simulations. *Curr. Opin. Struct. Biol.* **2014**, *24*, 98–105.

(41) Katava, M.; Stirnemann, G.; Zanatta, M.; Capaccioli, S.; Pachetti, M.; Ngai, K. L.; Sterpone, F.; Paciaroni, A. Critical structural fluctuations of proteins upon thermal unfolding challenge the Lindemann criterion. *Proc. Natl. Acad. Sci. U.S.A.* **2017**, *114*, 9361–9366.

(42) Timr, S.; Madern, D.; Sterpone, F. In *Computational Approaches for Understanding Dynamical Systems: Protein Folding and Assembly*; Strodel, B., Barz, B., Eds.; Progress in Molecular Biology and Translational Science; Academic Press, 2020; Vol. 170; pp 239 – 272.

(43) Prabhu, N. V.; Sharp, K. A. Heat Capacity in Proteins. *Annu. Rev. Phys. Chem.* **2005**, *56*, 521–548.

(44) Cooper, A. Protein Heat Capacity: An Anomaly that Maybe Never Was. *J. Phys. Chem. Lett.* **2010**, *1*, 3298–3304.

(45) Piana, S.; Donchev, A. G.; Robustelli, P.; Shaw, D. E. Water Dispersion Interactions Strongly Influence Simulated Structural Properties of Disordered Protein States. *J. Phys. Chem. B* **2015**, *119*, 5113–5123.